Maintenance of normal blood pressure is dependent on IP3R1-mediated regulation of eNOS

Qi Yuan[a,b,1], Jingyi Yang[a,b,c,1], Gaetano Santulli[a,b,1,2], Steven R. Reiken[a,b], Anetta Wronska[a,b], Mindy M. Kim[a], Brent W. Osborne[a], Alain Lacampagne[a,d], Yuxin Yin[c,2], and Andrew R. Marks[a,b,e,2]

[a]Department of Physiology and Cellular Biophysics, College of Physicians and Surgeons of Columbia University Medical Center, New York, NY 10032; [b]Wu Center for Molecular Cardiology, College of Physicians and Surgeons of Columbia University Medical Center, New York, NY 10032; [c]Institute of Systems Biomedicine, Department of Pathology, School of Basic Medical Sciences, Peking University Health Science Center, Beijing 100191, China; [d]INSERM U1046, CNRS UMR-9214, Université de Montpellier, 34295 Montpellier, France; and [e]Department of Medicine, Columbia University, New York, NY 10032

Contributed by Andrew R. Marks, June 2, 2016 (sent for review February 16, 2016; reviewed by Thomas M. Coffman and J. Kevin Foskett)

Endothelial cells (ECs) are critical mediators of blood pressure (BP) regulation, primarily via the generation and release of vasorelaxants, including nitric oxide (NO). NO is produced in ECs by endothelial NO synthase (eNOS), which is activated by both calcium (Ca^{2+})-dependent and independent pathways. Here, we report that intracellular Ca^{2+} release from the endoplasmic reticulum (ER) via inositol 1,4,5-trisphosphate receptor (IP3R) is required for Ca^{2+}-dependent eNOS activation. EC-specific type 1 1,4,5-trisphosphate receptor knockout ($IP3R1^{-/-}$) mice are hypertensive and display blunted vasodilation in response to acetylcholine (ACh). Moreover, eNOS activity is reduced in both isolated IP3R1-deficient murine ECs and human ECs following IP3R1 knockdown. IP3R1 is upstream of calcineurin, a Ca^{2+}/calmodulin-activated serine/threonine protein phosphatase. We show here that the calcineurin/nuclear factor of activated T cells (NFAT) pathway is less active and eNOS levels are decreased in IP3R1-deficient ECs. Furthermore, the calcineurin inhibitor cyclosporin A, whose use has been associated with the development of hypertension, reduces eNOS activity and vasodilation following ACh stimulation. Our results demonstrate that IP3R1 plays a crucial role in the EC-mediated vasorelaxation and the maintenance of normal BP.

hypertension | calcium | endothelium | IP3 receptor | eNOS

Hypertension (HTN) is a major cause of morbidity and mortality affecting millions of adults worldwide (1, 2). Globally, among the ∼17 million deaths caused by cardiovascular diseases, nearly half can be attributed to complications of HTN (3–9). In addition, vasodilator drugs that activate nitric oxide (NO) production have been used to treat HTN for decades (4, 10). Calcineurin (also known as protein phosphatase 2B), is a Ca^{2+}/calmodulin-activated serine/threonine protein phosphatase. Calcineurin inhibitors are first-line immunosuppressants used in organ transplantation (11, 12). However, calcineurin inhibition causes HTN in up to 70% of patients (13), and the exact underlying mechanisms are not fully understood.

Vascular endothelial cells (ECs), located at the interface between the vessel wall and blood, release vasorelaxants that influence vascular smooth muscle tone in response to mechanical (e.g., shear stress) and biochemical stimuli (14, 15). These stimuli induce a rapid increase in intracellular Ca^{2+} ($[Ca^{2+}]_i$) in ECs activating Ca^{2+}-dependent signaling pathways, resulting in release of endothelium-derived relaxing factors, including NO (14, 16–19). Mice lacking endothelial nitric oxide synthase (eNOS) develop severe HTN (20). However, how eNOS is regulated in vivo remains essentially unclear. The modulation of both plasma membrane Ca^{2+} entry and endoplasmic reticulum (ER) Ca^{2+} release is critical in EC function (21, 22).

Moreover, recent meta-analysis and genome-wide association studies in hypertensive individuals have linked type 1 1,4,5-trisphosphate receptor (*IP3R1*), a major $[Ca^{2+}]_i$ release channel (23, 24), to high blood pressure (BP) (25, 26). On these grounds, we sought to investigate in detail the functional role of the IP3R1/Ca^{2+}/calcineurin/nuclear factor of activated T cells (NFAT)/eNOS pathway in BP regulation.

Results and Discussion

Generation and Characterization of Endothelium-Specific IP3R1 Knockout Mice. Previous studies have reported embryonic lethality in calcineurin B mutant and NFATc3 and NFATc4 double-knockout mice models (27). Furthermore, there are three isoforms of calcineurin A and one of calcineurin B in ECs (28) plus four isoforms of NFAT (29). Thus, genetic approaches to elucidate the functions of these molecules are problematic. Therefore, to dissect the IP3R1/Ca^{2+}/calcineurin/NFAT/eNOS pathway, and to understand better the molecular mechanisms underlying BP regulation, we examined the role of IP3R1 in the Ca^{2+}-dependent eNOS activation in ECs. We generated EC-specific IP3R1 knockout (EC $IP3R1^{-/-}$) mice resulting from crosses of floxed IP3R1 mice with $Tie2^{Cre}$ mice (Fig. S1 *A* and *B*). IP3R1 expression was significantly reduced in vascular ECs isolated from EC $IP3R1^{-/-}$ mice compared with mice harboring the $IP3R1^{flox/flox}$ allele ($IP3R1^{fl/fl}$) (Fig. S1*C*). In contrast, levels of mRNA encoding the two other isoforms of IP3R, IP3R2 and IP3R3, did not exhibit compensatory up-regulation in vascular ECs from EC $IP3R1^{-/-}$ mice (Fig. S1*C*). Immunofluorescence analysis did not detect IP3R1 protein in vascular ECs from EC $IP3R1^{-/-}$ mice (Fig. S1*D*). Additionally, EC $IP3R1^{-/-}$ mice exhibited normal embryonic development (Fig. S2).

Effect of Endothelial Disruption on BP. Strikingly, mean arterial pressure (measured using radiotelemetry) was significantly elevated in freely ambulating EC $IP3R1^{-/-}$ mice by 3 mo of age (Fig. 1*A*). These findings were confirmed by measuring BP using a Millar catheter (Fig. S3*A*) or tail-cuff (Fig. S3*B*). At 6 mo of age, chronic HTN resulted in cardiac enlargement and overall reduced function in EC $IP3R1^{-/-}$ mice (Table S1). Mesenteric arteries exhibited markedly thickened tunica media (Fig. S4 *A* and *B*) with an increased media/lumen ratio (Fig. S4*C*) in EC $IP3R1^{-/-}$ mice.

Significance

In this study, we demonstrate that type 1 inositol 1,4,5-trisphosphate receptor channels are critically involved in the activation of the calcineurin/nuclear factor of activated T cells (NFAT)/endothelial nitric oxide synthase signaling pathway in endothelial cells. This pathway plays an essential role in the maintenance of normal blood pressure, with important implications in the clinical scenario.

Author contributions: A.R.M. conceived of the study; G.S. and A.R.M. designed experiments; G.S. performed experiments; Q.Y. designed and performed ex vivo experiments; J.Y. performed in vitro experiments; S.R.R. and A.W. contributed new reagents/analytic tools; G.S., M.M.K., B.W.O., A.L., Y.Y., and A.R.M. analyzed data; and Q.Y., J.Y., G.S., and A.R.M. wrote the paper.

Reviewers: T.M.C., Duke University; and J.K.F., University of Pennsylvania.

The authors declare no conflict of interest.

[1]Q.Y, J.Y, and G.S. contributed equally to this work.

[2]To whom correspondence may be addressed. Email: gs2620@cumc.columbia.edu, yinyuxin@hsc.pku.edu.cn, or arm42@columbia.edu.

This article contains supporting information online at www.pnas.org/lookup/suppl/doi:10.1073/pnas.1608859113/-/DCSupplemental.

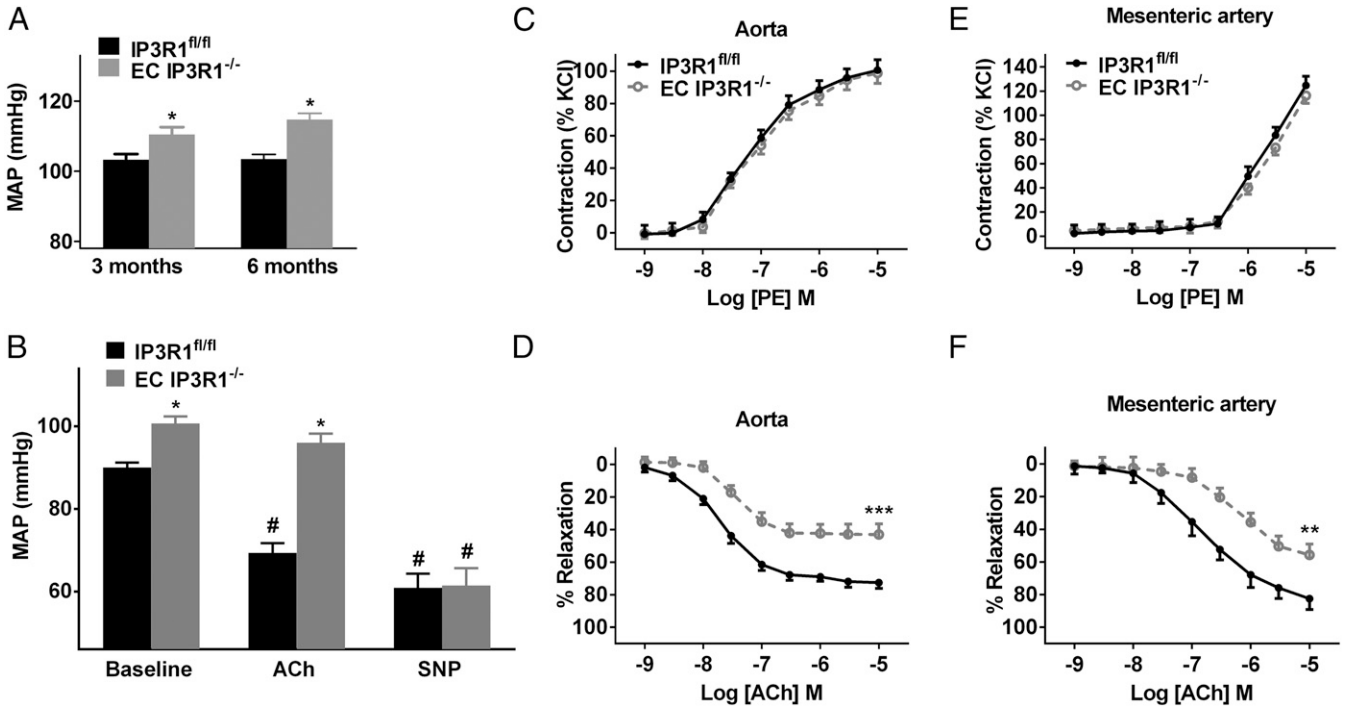

Fig. 1. Effect of endothelial disruption of IP3R1 in ECs on BP and vascular reactivity. (*A*) Mean arterial pressure (MAP) recorded by radiotelemetry in at least seven IP3R1$^{fl/fl}$ and EC IP3R1$^{-/-}$ mice. (*B*) MAP measured by an intra-arterial Millar catheter in IP3R$^{fl/fl}$ and EC IP3R1$^{-/-}$ mice in response to ACh and SNP injection. *$P < 0.05$ vs. IP3Rfl/fl mice; #$P < 0.05$ vs. baseline ($n \geq 6$ mice per each group) by Student's *t* test. (C) Vasoconstrictor reactivity to the α1-adrenoreceptor agonist phenylephrine (PE) in aorta arteries in IP3R1$^{fl/fl}$ and EC IP3R1$^{-/-}$ mice. (*D*) Endothelium-dependent relaxation to ACh in aorta arteries. There was a significant decrease in potency (rightward shift) of the concentration response curve to ACh in the aortic arteries of EC IP3R1$^{-/-}$ mice. ***$P < 0.001$ vs. IP3R1$^{fl/fl}$ mice by Student's *t* test. (*E*) Vasoconstrictor reactivity to PE in mesenteric arteries. (*F*) Endothelium-dependent relaxation to ACh in mesenteric arteries. There was a significant decrease in potency (rightward shift) of the concentration response curve to ACh in the mesenteric arteries of EC IP3R1$^{-/-}$ mice. Data are presented as mean ± SEM (n = 12–20 rings from six mice per group for aorta arteries, n = 8 for isolated mesenteric arteries). **$P < 0.01$ vs. IP3R1$^{fl/fl}$ mice by Student's *t* test.

In addition, both cardiac fibrosis and renal fibrosis were augmented in 6-mo-old EC IP3R1$^{-/-}$ mice (Fig. S4 *D* and *E*). Taken together, these data show that EC IP3R1$^{-/-}$ mice have a chronic hypertensive phenotype with typical target-organ damage, including the heart, kidney, and vasculature. Further studies are needed to investigate in detail the potential involvement of the regulation of sodium excretion in the kidney and other renal pathways (30, 31).

Defective Vasodilation in EC IP3R1$^{-/-}$ Mice. EC IP3R1$^{-/-}$ mice exhibited a blunted vasodilatory response to i.v. ACh (Fig. 1*B*). However, injection of the endothelium-independent vasodilator sodium nitroprusside (SNP; an NO donor) caused an equivalent BP reduction in both IP3R1$^{fl/fl}$ and EC IP3R1$^{-/-}$ mice (Fig. 1*B*), indicating that the vasodilatory response to NO was intact.

Responses to the vasoconstrictor phenylephrine (an α_1-adrenoreceptor agonist) were intact in aortas and mesenteric arteries from both IP3R1$^{fl/fl}$ and EC IP3R1$^{-/-}$ mice (Fig. 1 *C* and *E*). However, the ACh-induced aortic relaxation was markedly blunted (by ∼41%) in EC IP3R1$^{-/-}$ mice compared with IP3R1$^{fl/fl}$ mice (Fig. 1*D*). Responses to the Ca^{2+} ionophore A23187 were also markedly impaired (by ∼23%) in EC IP3R1$^{-/-}$ mice (Fig. S5). Similarly, there was a significant reduction in the response to ACh (Fig. 1*F*) in EC IP3R1$^{-/-}$ mesenteric arteries. Importantly, responses to SNP were comparable between IP3R1$^{fl/fl}$ and EC IP3R1$^{-/-}$ mice in both vascular districts (Fig. S6 *A* and *B*).

Diminished ACh-Induced Ca^{2+}-Dependent NO Production in EC IP3R1$^{-/-}$ Mice. To confirm that the observed blunted vasodilation was due to deficient IP3R1-mediated ER Ca^{2+} release, we examined the ACh-induced Ca^{2+} response in isolated aortic ECs. Addition of ACh elicited a rapid dose-dependent increase in $[Ca^{2+}]_i$ in IP3R1$^{fl/fl}$ ECs that was significantly reduced in IP3R1$^{-/-}$ ECs. Incubation of ECs with Xestospongin C (Xec; an IP3R inhibitor) also inhibited the rise in $[Ca^{2+}]_i$ in response to ACh in both groups (Fig. 2*B*). Similar results were obtained using a second IP3R inhibitor (2-aminoethoxydiphenyl borate; Fig. S7). These genetic and pharmacological data indicate that IP3R1 activation contributes to the ACh-induced $[Ca^{2+}]_i$ increase in vascular ECs. The increase in ACh-induced EC NO was blunted in EC IP3R1$^{-/-}$ mice (Fig. 2*C*), and NO production in control mice was reduced by Xec or L-NG-nitroarginine methyl ester (L-NAME) (Fig. 2*D*), indicating that IP3R1-mediated ER Ca^{2+} plays a pivotal role in EC NO generation.

EC NO is produced primarily by eNOS following agonist stimulation, and eNOS activity is dependent on Ca^{2+}-calmodulin (17, 32). Under basal conditions, eNOS activity in ECs isolated from EC IP3R1$^{-/-}$ mice was reduced compared with eNOS activity in ECs from IP3R1$^{fl/fl}$ mice (Fig. 2*E*). ACh (10 μM) increased eNOS activity by 2.6-fold in IP3R1$^{fl/fl}$ mice, whereas such an increase was not observed in EC IP3R1$^{-/-}$ mice (Fig. 2*E*).

Defective eNOS Activity Due to Decreased Expression and Phosphorylation. eNOS activity is determined both by basal protein level and by enzymatic activity, which is regulated by phosphorylation (33). HTN was associated with reduced eNOS protein in EC IP3R1$^{-/-}$ mesenteric arteries (Fig. 3*A*), as well as attenuated eNOS phosphorylation at Ser^{1176} in response to ACh stimulation (Fig. 3*A*). Moreover, phosphorylation of eNOS at Thr^{494}, which is an inhibitory site (34), was increased in EC IP3R1$^{-/-}$ mesenteric arteries (Fig. 3*B*). IP3R1-deficient human ECs, generated by transfecting IP3R1 siRNAs into human umbilical vein endothelial

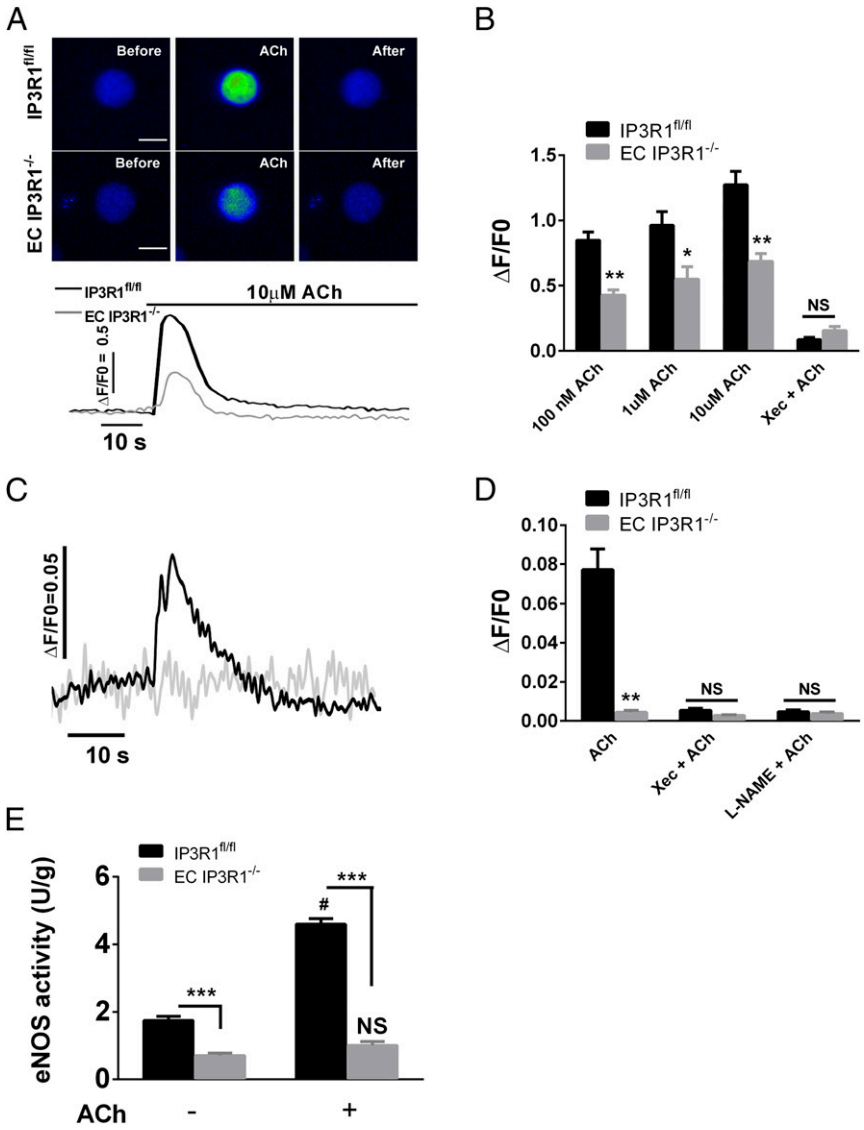

Fig. 2. ACh-induced Ca^{2+} increase and NO production in isolated aortic ECs. (*A*) Representative images (*Upper*) and traces (*Lower*) of endothelial Ca^{2+} responses to ACh measured with the fluorescence Ca^{2+} indicator Fluo-4. (Scale bars: 20 μm.) (*B*) Summarized data regarding endothelial Ca^{2+} increase. Data are presented as mean ± SEM (n = 30–40 cells from six mice per each group). $^{*}P < 0.05$; $^{**}P < 0.01$. NS, not significant. (*C*) Representative traces of endothelial NO increase in response to ACh. (*D*) Summarized data of maximal endothelial NO fluorescence. Data are presented as mean ± SEM (n = 20–30 cells from six mice per group). $^{**}P < 0.01$. (*E*) NOS activity measured in isolated aortic ECs with (+) or without (–) 10 μM ACh treatment at 37 °C for 10 min. Data are shown as mean ± SEM of at least three independent experiments. $^{***}P < 0.001$ vs. $IP3R1^{fl/fl}$ ECs within the same group; $^{\#}P < 0.001$ vs. untreated $IP3R1^{fl/fl}$ ECs; NS, not significant vs. untreated EC $IP3R1^{-/-}$ ECs (all by Student's t test).

cells (HUVECs), exhibited an ~50% decrease in eNOS protein (Fig. 3*C*) and mRNA (Fig. 3*D*).

Effects of IP3R1 Deletion on the Calcineurin/NFAT Pathway in ECs. The calcineurin/NFAT pathway has been identified as being located downstream of the angiotensin II type 2 receptor to promote eNOS expression in the myocardium, where it is believed to protect against cardiac hypertrophy (35). We examined NFAT translocation to the nucleus to determine whether NFAT might be a regulator of eNOS expression in ECs. Indeed, nuclear translocation of NFAT was reduced in response to ACh stimulation in both IP3R1 knockdown HUVECs (Fig. 3 *E* and *F*) and isolated IP3R1-deficient ECs (Fig. S8). Taken together, these data provide a mechanism for the reduced eNOS levels observed in IP3R1-deficient ECs whereby decreased ER Ca^{2+} release impairs activation of downstream calcineurin/NFAT signaling.

The calcineurin inhibitor cyclosporin A (CsA) significantly reduced ACh-induced vasodilation, but did not reduce SNP-mediated vasodilation in $IP3R1^{fl/fl}$ mice (Fig. S9). Preincubation of HUVECs with CsA for 1 h blocked ACh-induced NFAT translocation (Fig. 3 *E* and *F*). eNOS activation by ACh was also inhibited by CsA in a dose-dependent manner (Fig. 3*G*). These data suggest that the IP3R1/calcineurin/NFAT signaling pathway plays a key role in ACh-induced eNOS activity in vascular ECs.

Stimulation of muscarinic M_1 receptors in ECs by ACh activates phospholipase C-γ_1, resulting in IP3 production and IP3R-mediated Ca^{2+} release from the ER (36). Our data show that increased $[Ca^{2+}]_i$, in turn, activates the calcineurin/NFAT pathway, resulting in increased eNOS expression and activity in vascular ECs (Fig. 4). Although Ca^{2+}-induced eNOS activation appears to be an important pathway for vasodilation, we cannot rule out the involvement of other vasodilators [e.g., prostaglandin

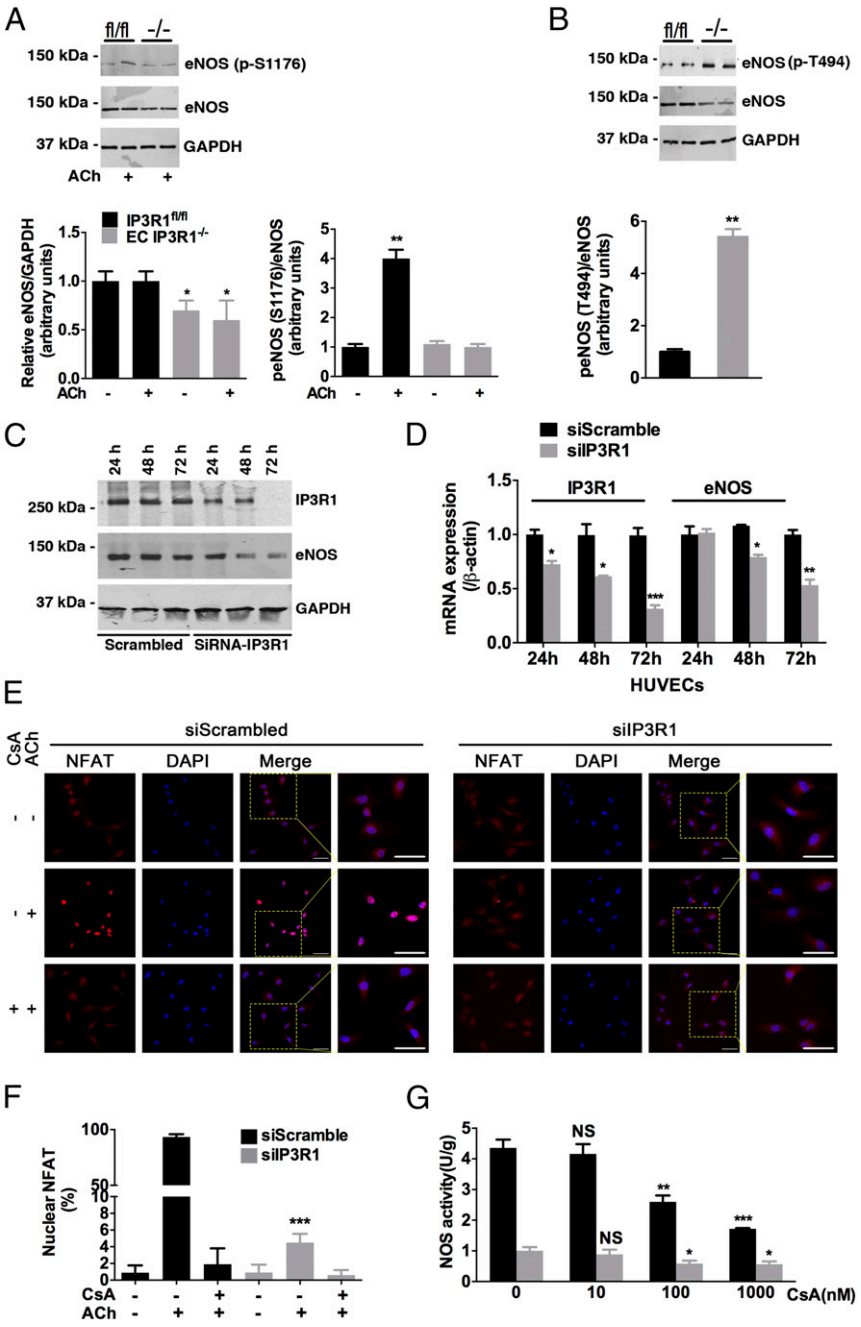

Fig. 3. Calcineurin in eNOS regulation. (*A*) Expression of eNOS and phosphorylation of eNOS at Ser1176 (p-S1176) in lysates from mesenteric arteries prepared under basal conditions or after 30-min ACh incubation in IP3R1$^{fl/fl}$ and EC IP3R1$^{-/-}$ mice. The graph shows the densitometric evaluation ($n = 3$). *$P <$ 0.05; **$P < 0.01$. (*B*) Phosphorylation of eNOS at Thr494 (p-T494) in lysates from mesenteric arteries in IP3R1$^{fl/fl}$ and EC IP3R1$^{-/-}$ mice. Data are presented as mean ± SEM of three independent experiments. **$P < 0.01$. (*C*) Immunoblots conducted in HUVECs transfected with scrambled or IP3R1-specific siRNAs. Cells were harvested 24 h, 48 h, and 72 h after transfection. (*D*) Relative IP3R1 and eNOS mRNA levels were measured by real-time RT-quantitative PCR in HUVECs after indicated times of transfection. β-Actin was used as an internal control. (*A–D*) *$P < 0.05$; **$P < 0.01$; ***$P < 0.001$ vs. scrambled by Student's *t* test. (*E*) Representative immunofluorescence images of NFAT intracellular localization in transfected HUVECs, with or without CsA (1 μM, 1 h) and ACh (10 μM, 10 min) treatment. NFAT, red; DAPI, blue. (Magnification: 20×.) (Scale bars: 20 μm.) (*F*) Quantification of cells with nuclear-translocated NFAT. More than 30 cells were calculated for each condition, and data are presented as mean ± SEM of three independent experiments. ***$P < 0.001$ vs. siScrambled treated with ACh only, analyzed by Student's *t* test. (*G*) Isolated aortic ECs were pretreated with gradient concentrations (0, 10, 100, and 1,000 nM) of CsA at 37 °C for 1 h, followed by ACh stimulation and NOS activity measurement as described in Fig. 2*E*. *$P < 0.05$; **$P < 0.01$; ***$P < 0.001$; NS, not significant vs. 0 nM CsA-treated cells of respective group, analyzed by Student's *t* test.

I2, endothelium-derived hyperpolarizing factor (EDHF)], particularly in mesenteric arteries, where EDHF is a major vasodilator downstream of increased $[Ca^{2+}]_i$ (18). In addition, eNOS posttranslational modification at other sites upon ACh stimulation may contribute to the low activity in EC IP3R1$^{-/-}$ mice (Fig. 3 *A* and *B*). Phosphorylation of eNOS at Ser^{1176} is a positive regulator of eNOS activity and is mediated by Ca^{2+}/calmodulin/calmodulin-dependent protein kinase II (CaMKII) cascade,

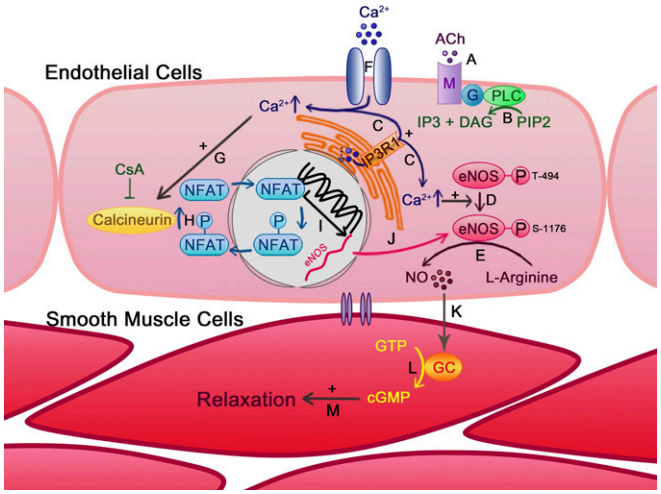

Fig. 4. Role of IP3R1 in ACh-induced vasodilation. ACh binds and activates muscarinic receptor (M) on the EC membrane (A), which leads to the production of diacylglycerol (DAG) and IP3 (B). (C) IP3 activates IP3R1 on the ER membrane to induce Ca^{2+} release from the ER store, resulting in the elevation of $[Ca^{2+}]_i$. Increased $[Ca^{2+}]_i$ up-regulates eNOS activity by modifying the eNOS protein phosphorylation status (D) and promotes NO production from L-arginine (E). (F) Ca^{2+} reduction in the ER store induces extracellular Ca^{2+} entry through calcium channels. $[Ca^{2+}]_i$ increase can also activate calcineurin (G), which dephosphorylates NFAT and promotes NFAT nuclear translocation (H). (I) NFAT induces eNOS gene transcription and translocates back into the cytoplasm. (J) eNOS protein level is transcriptionally up-regulated by an IP3R1-mediated Ca^{2+}-release–dependent calcineurin/NFAT mechanism. EC-generated NO diffuses into adjacent smooth muscle cells (K) and activates guanylyl cyclase (GC) to generate cGMP from GTP (L), leading to smooth muscle relaxation (M).

whereas the phosphorylation of Thr^{494} inhibits eNOS catalytic activity (33). Calcineurin has been reported to dephosphorylate eNOS at Ser^{116} in human and bovine ECs (37); however, this site shows very low homology in murine EC eNOS. Further investigations are warranted to explore in detail the role of IP3R1 in the modulation of EC bioenergetics (38), which might contribute to the observed hypertensive phenotype.

Taken together, our results demonstrate that EC IP3R1 channels are crucial for the activation of the calcineurin/NFAT/eNOS signaling pathway, which, in turn, plays a fundamental role in the maintenance of normal BP.

Materials and Methods

Animal Studies. Exon 4 of the gene encoding for IP3R1 was targeted by flanking it with loxP sites (Fig. S1*A*). Methodologies for the generation of embryonic stem cell-derived embryos have been described elsewhere (39). $IP3R1^{fl/fl}$ mice were bred with Tie2-Cre transgenic mice to obtain an EC-specific ablation of IP3R1 (EC IP3R1 KO). Genotypes were verified by PCR (Fig. S1*B* and Table S2). All mice were backcrossed into the C57BL/6 background for >10 generations. BP was recorded via radiotelemetry, Millar catheter, and tail-cuff, as previously described (39). Vascular reactivity of mouse thoracic aortic and mesenteric arterial ring preparations was determined following established protocols (40).

A detailed description of materials and methods can be found in *SI Materials and Methods*.

Ethical Approval. All studies were performed according to protocols approved by the Institutional Animal Care and Use Committee of Columbia University and according to NIH guidelines. All experiments were conducted by operators who were blinded to the genotypes of the animals. No samples, mice, or data points were excluded from the reported analyses.

Statistics. All results are presented as mean ± SEM. Statistical analysis was performed using an unpaired two-tailed Student's *t* test unless otherwise indicated. *P* values <0.05 were considered significant.

ACKNOWLEDGMENTS. We thank Frances Forrester, Bi-Xing Chen, and Matthew J. Borok for technical assistance. This work was supported by grants from the NIH [Grant K99DK107895 (to G.S.), Grant R25 NS076445 (to M.M.K.), Grant T32GM008464 (to B.W.O.), and Grants R01AR060037 and R01HL061503 (to A.R.M.)], and a Schaeffer Research fellowship (to A.L.). J.Y. was supported by the Chinese Scholarship Council.

1. Santulli G (2013) Epidemiology of cardiovascular disease in the 21st century: Updated numbers and updated facts. *J Cardiovasc Dis* 1(1):1–2.
2. Blacher J, Levy BI, Mourad JJ, Safar ME, Bakris G (February 5, 2016) From epidemiological transition to modern cardiovascular epidemiology: Hypertension in the 21st century. *Lancet*, 10.1016/S0140-6736(16)00002-7.
3. Lackland DT, Weber MA (2015) Global burden of cardiovascular disease and stroke: Hypertension at the core. *Can J Cardiol* 31(5):569–571.
4. Santulli G, Trimarco B, Iaccarino G (2013) G-protein-coupled receptor kinase 2 and hypertension: Molecular insights and pathophysiological mechanisms. *High Blood Press Cardiovasc Prev* 20(1):5–12.
5. Hansson JH, et al. (1995) Hypertension caused by a truncated epithelial sodium channel gamma subunit: Genetic heterogeneity of Liddle syndrome. *Nat Genet* 11(1):76–82.
6. Lanni F, et al. (2007) The Pl(A1/A2) polymorphism of glycoprotein IIIa and cerebrovascular events in hypertension: Increased risk of ischemic stroke in high-risk patients. *J Hypertens* 25(3):551–556.
7. Coffman TM (2014) The inextricable role of the kidney in hypertension. *J Clin Invest* 124(6):2341–2347.
8. Lifton RP (1996) Molecular genetics of human blood pressure variation. *Science* 272(5262):676–680.
9. Iaccarino G, et al. (2004) AKT participates in endothelial dysfunction in hypertension. *Circulation* 109(21):2587–2593.
10. Koch-Weser J (1974) Vasodilator drugs in the treatment of hypertension. *Arch Intern Med* 133(6):1017–1027.
11. van Gelder T, van Schaik RH, Hesselink DA (2014) Pharmacogenetics and immunosuppressive drugs in solid organ transplantation. *Nat Rev Nephrol* 10(12):725–731.
12. Rodríguez-Perálvarez M, De la Mata M, Burroughs AK (2014) Liver transplantation: Immunosuppression and oncology. *Curr Opin Organ Transplant* 19(3):253–260.
13. Zbroch E, Małyszko J, Myśliwiec M, Przybyłowski P, Durlik M (2012) Hypertension in solid organ transplant recipients. *Ann Transplant* 17(1):100–107.
14. Palmer RM, Ashton DS, Moncada S (1988) Vascular endothelial cells synthesize nitric oxide from L-arginine. *Nature* 333(6174):664–666.
15. Rapoport RM, Draznin MB, Murad F (1983) Endothelium-dependent relaxation in rat aorta may be mediated through cyclic GMP-dependent protein phosphorylation. *Nature* 306(5939):174–176.
16. Luksha L, Agewall S, Kublickiene K (2009) Endothelium-derived hyperpolarizing factor in vascular physiology and cardiovascular disease. *Atherosclerosis* 202(2):330–344.
17. Santulli G, et al. (2012) CaMK4 gene deletion induces hypertension. *J Am Heart Assoc* 1(4):e001081.
18. Chataigneau T, et al. (1999) Acetylcholine-induced relaxation in blood vessels from endothelial nitric oxide synthase knockout mice. *Br J Pharmacol* 126(1):219–226.
19. Matoba T, et al. (2000) Hydrogen peroxide is an endothelium-derived hyperpolarizing factor in mice. *J Clin Invest* 106(12):1521–1530.
20. Shesely EG, et al. (1996) Elevated blood pressures in mice lacking endothelial nitric oxide synthase. *Proc Natl Acad Sci USA* 93(23):13176–13181.
21. Taylor MS, Francis M (2014) Decoding dynamic Ca(2+) signaling in the vascular endothelium. *Front Physiol* 5:447.
22. Kochukov MY, Balasubramanian A, Abramowitz J, Birnbaumer L, Marrelli SP (2014) Activation of endothelial transient receptor potential C3 channel is required for small conductance calcium-activated potassium channel activation and sustained endothelial hyperpolarization and vasodilation of cerebral artery. *J Am Heart Assoc* 3(4):e000913.
23. Santulli G, Marks AR (2015) Essential roles of intracellular calcium release channels in muscle, brain, metabolism, and aging. *Curr Mol Pharmacol* 8(2):206–222.
24. Yang J, et al. (2002) Identification of a family of calcium sensors as protein ligands of inositol trisphosphate receptor Ca(2+) release channels. *Proc Natl Acad Sci USA* 99(11):7711–7716.
25. Marques FZ, Campain AE, Yang YH, Morris BJ (2010) Meta-analysis of genome-wide gene expression differences in onset and maintenance phases of genetic hypertension. *Hypertension* 56(2):319–324.
26. Edwards JS, et al. (2014) Integrated statistical and pathway approach to next-generation sequencing analysis: A family-based study of hypertension. *BMC Proc* 8(Suppl 1):S104.
27. Graef IA, Chen F, Chen L, Kuo A, Crabtree GR (2001) Signals transduced by Ca(2+)/calcineurin and NFATc3/c4 pattern the developing vasculature. *Cell* 105(7):863–875.
28. Rinne A, Banach K, Blatter LA (2009) Regulation of nuclear factor of activated T cells (NFAT) in vascular endothelial cells. *J Mol Cell Cardiol* 47(3):400–410.
29. Zetterqvist AV, et al. (2015) Nuclear factor of activated T cells is activated in the endothelium of retinal microvessels in diabetic mice. *J Diabetes Res* 2015:428473.
30. Gurley SB, et al. (2011) AT1A angiotensin receptors in the renal proximal tubule regulate blood pressure. *Cell Metab* 13(4):469–475.
31. Crowley SD, Gurley SB, Coffman TM (2007) AT(1) receptors and control of blood pressure: The kidney and more.... *Trends Cardiovasc Med* 17(1):30–34.
32. Ciccarelli M, et al. (2014) CaMKII protects MKP-1 from proteasome degradation in endothelial cells. *Cell Signal* 26(10):2167–2174.

33. Rafikov R, et al. (2011) eNOS activation and NO function: Structural motifs responsible for the posttranslational control of endothelial nitric oxide synthase activity. *J Endocrinol* 210(3):271–284.
34. Nguyen H, et al. (2013) Interleukin-17 causes Rho-kinase-mediated endothelial dysfunction and hypertension. *Cardiovasc Res* 97(4):696–704.
35. Ritter O, et al. (2003) AT2 receptor activation regulates myocardial eNOS expression via the calcineurin-NF-AT pathway. *FASEB J* 17(2):283–285.
36. Adams DJ, Barakeh J, Laskey R, Van Breemen C (1989) Ion channels and regulation of intracellular calcium in vascular endothelial cells. *FASEB J* 3(12):2389–2400.
37. Kou R, Greif D, Michel T (2002) Dephosphorylation of endothelial nitric-oxide synthase by vascular endothelial growth factor. Implications for the vascular responses to cyclosporin A. *J Biol Chem* 277(33):29669–29673.
38. Cárdenas C, et al. (2010) Essential regulation of cell bioenergetics by constitutive InsP3 receptor Ca2+ transfer to mitochondria. *Cell* 142(2):270–283.
39. Santulli G, Xie W, Reiken SR, Marks AR (2015) Mitochondrial calcium overload is a key determinant in heart failure. *Proc Natl Acad Sci USA* 112(36):11389–11394.
40. Santulli G, et al. (2014) A selective microRNA-based strategy inhibits restenosis while preserving endothelial function. *J Clin Invest* 124(9):4102–4114.
41. Santulli G, et al. (2009) In vivo properties of the proangiogenic peptide QK. *J Transl Med* 7:41.
42. Xie W, et al. (2013) Imaging atrial arrhythmic intracellular calcium in intact heart. *J Mol Cell Cardiol* 64:120–123.
43. Santulli G, et al. (2015) Calcium release channel RyR2 regulates insulin release and glucose homeostasis. *J Clin Invest* 125(5):1968–1978.
44. Yuan Q, et al. (2014) Functional role of Calstabin2 in age-related cardiac alterations. *Sci Rep* 4:7425.
45. Umanskaya A, et al. (2014) Genetically enhancing mitochondrial antioxidant activity improves muscle function in aging. *Proc Natl Acad Sci USA* 111(42):15250–15255.
46. Xie W, et al. (2015) Mitochondrial oxidative stress promotes atrial fibrillation. *Sci Rep* 5:11427.
47. Santulli G, et al. (2012) Age-related impairment in insulin release: The essential role of β(2)-adrenergic receptor. *Diabetes* 61(3):692–701.

Supporting Information

Yuan et al. 10.1073/pnas.1608859113

SI Materials and Methods

Targeted Deletion of IP3R1 in ECs. Exon 4 of the gene encoding for IP3R1 was targeted by flanking it with loxP sites (Fig. S1*A*). Detailed methodologies for the generation of embryonic stem cell-derived embryos have been described elsewhere (39). Mice harboring the $IP3R1^{fl/fl}$ allele were bred with Tie2-Cre transgenic mice to obtain an EC-specific ablation of IP3R1 (EC IP3R1 KO). Genotypes were verified by PCR (Fig. S1*B*). All mice were backcrossed into the C57BL/6 background for >10 generations. All animal studies were performed according to protocols approved by the Institutional Animal Care and Use Committee of Columbia University and according to NIH guidelines. All in vivo and in vitro experiments were conducted on male mice by operators who were blinded to the genotypes of the animals. No samples, mice, or data points were excluded from the reported analyses.

Radiotelemetric BP Recording. BP was recorded in conscious, freely moving mice using radiotelemetric transmitters (TA11PA-C10; Data Sciences International) implanted into the aortic arch (39). After 10 d of recovery, BP was recorded for 24 h in mice left undisturbed and maintained on a 12-h light/12-h dark cycle. Data were acquired for 2 min every 15 min, and the average values for MAP were calculated for every time point.

BP Measurement by Millar Catheter. BP was measured as previously described (17). Briefly, mice were anesthetized by isoflurane inhalation and maintained by mask ventilation. Direct BP and heart rate measurements were performed with the use of a 1.0-French Mikro-Tip catheter (SPR1000; Millar Instruments), which was advanced through the right external carotid artery and placed in the descending aorta. After implantation, the catheter was connected to a transducer (Gould Instruments Systems) to record BP and heart rate for 15 min.

BP Measurement by Tail-Cuff. BP was measured using a tail-cuff method that relies on volume/pressure recording technology (Coda 6; Kent Scientific Corporation). BP was measured each day at the same time.

Vascular Reactivity ex Vivo. The vascular reactivity of mouse thoracic aortic and mesenteric arterial ring preparations was determined as previously described and validated (40, 41). Briefly, 3- to 6-mo-old mice were killed, and the mesentery artery and thoracic aorta were rapidly removed and dissected in ice-cold Krebs solution (119 mM NaCl, 4.7 mM KCl, 2.5 mM $CaCl_2$, 1 mM $MgCl_2$, 25 mM $NaHCO_3$, 1.2 mM KH_2PO_4, and 11 mM D-glucose). Mesenteric artery rings and thoracic aorta segments were mounted in a Multi Myograph System (510; Danish Myo Technology A/S), and modifications in arterial tone were recorded. Cumulative concentration response curves to phenylephrine (PE) were assessed in order to evaluate the contractility response. To evaluate vasorelaxation and the integrity of the endothelium layer, cumulative concentration response curves to ACh (1 nM to 30 μM), A23187 (1 nM to 10 μM), and SNP (1 nM to 10 μM) were tested on PE (1 μM) precontracted rings.

EC Isolation. After euthanization, murine aortas were quickly harvested, removed from adipose and connective tissues, cut through the longitudinal axis, and suspended in 1 mL of dissociation solution [55 mM NaCl, 80 mM Na-glutamate, 6 mM KCl, 2 mM $MgCl_2$, 0.1 mM $CaCl_2$, 10 mM glucose, and 10 mM Hepes (pH 7.3)] containing 0.5 mg/mL neutral protease and 1 mg/mL elastase (Worthington). After digestion for 1 h at 37 °C, type 1 collagenase (Worthington) was added to the dissociation solution to a final concentration of 0.5 mg/mL, and digestion was continued for an additional 2 min at 37 °C. Aortas were then transferred to 1 mL of Ca^{2+}-free dissociation solution, and cells were released by pipetting gently for about 10 times. Isolated ECs were collected by centrifugation at 100 × *g* for 1 min.

Ca^{2+} Imaging. Confocal Ca^{2+} imaging of ECs was performed as previously described (42, 43). Briefly, isolated aortic ECs were incubated with 10 μM Fura-2:00 AM (Invitrogen) in normal Tyrode's solution, containing 135 mM NaCl, 4 mM KCl, 1.8 mM $CaCl_2$, 1 mM $MgCl_2$, 10 mM Hepes, 1.2 mM $NaH_2PO_4 \bullet 2H_2O$, and 10 mM glucose (pH 7.36) adjusted with NaOH for 15 min at room temperature. After loading, the cells were washed several times and transferred to a recording chamber. Confocal imaging was performed by excitation with a 488-nm light from the argon laser of a Zeiss 5 live inverted confocal microscope (63× oil immersion lens). Data were analyzed using Image J software (NIH).

Measurement of NO by DAF-FM Dye. Isolated aortic ECs were loaded with 20 μM NO-sensitive fluorescent dye: DAF-FM (4-amino-5-methylamino-2, 7-difluorofluorescein diacetate; Invitrogen) for 30 min at room temperature. Cells were then resuspended in Tyrode's solution (1.8 mM Ca^{2+}). DAF fluorescence confocal images were acquired in the *x*–*y* mode (Zeiss 5 live inverted confocal microscope, 63× oil immersion lens), with 488-nm excitation with an argon ion laser and a 510- to 530-nm emission filter. The fluorescence values were corrected for the background fluorescence from a region of the image without cells (F − F0), and the fluorescence/background ratio $[(F - F_0)/F_0]$ was calculated. All images were processed and analyzed using Fiji software.

Histology. Embryos or tissues were fixed in 10% formaldehyde overnight and processed for paraffin embedding. Hematoxylin and eosin (H&E) staining was performed on 7-μm sections following standard protocols (41). Fibrosis was evaluated by Masson's trichrome staining (Sigma) according to the manufacturer's protocol. Mesenteric artery morphometric analysis was performed with ImageJ software by measuring the circumference of the external elastic lamina and internal elastic lamina. Media thickness and the media/lumen ratio were calculated to evaluate vessel remodeling as described (40).

Immunoblotting. Mouse mesenteric arteries were harvested, quickly rinsed in PBS, immediately frozen in liquid nitrogen, and stored at −80 °C. Frozen tissues or HUVECs were homogenized in 150 mM NaCl, 25 mM Tris·HCl (pH 7.5), 5 mM EDTA, 1% Nonidet P-40, 0.4% deoxycholic acid, 1 mM Na_3VO_4, and complete protease inhibitors. Protein concentrations were determined using the bicinchoninic acid assay (BCA) assay. Ten to 20 μg of protein was size-fractionated on SDS/PAGE and immunoblotted. Immunoblotting was performed as previously described and validated (43–46) using the following antibodies: eNOS (catalog no. 610297; BD Biosciences), phosphor-eNOS (Thr-495, catalog no. 9574s; Cell Signaling Technology), phospho-eNOS (Ser-1177, catalog no. 9571s; Cell Signaling Technology), and GAPDH (catalog no. 2118; Cell Signaling Technology).

Immunofluorescence. Paraffin-embedded tissues were deparaffinized, hydrated, and antigen-retrieved before immunostaining with IP3R1 antibody (1:100). Isolated aortic ECs were seeded on

35-mm glass-bottomed dishes (MatTek Corporation) precoated with poly-L-lysine solution (Sigma) and stained with NFATc3 antibody (1:50; Santa Cruz Biotechnology). Cy3-labeled secondary antibody (1:1,000; Abcam) was incubated for 1 h at room temperature, followed by mounting with SlowFade Gold antifade reagent with DAPI (Thermo Fisher Scientific). Pictures were captured with a Zeiss 5 live inverted confocal microscope (63× oil immersion lens) (40).

RT-Quantitative PCR. Total RNAs were extracted using TRIzol (Invitrogen) and subjected to synthesize cDNA (RR047A; Takara). SYBR *Premix Ex* Taq II (RR820A; Takara) was used to quantify corresponding gene expression according to the manufacturer's instructions. Detailed primer sequences are listed in Table S1. All reactions were run in triplicate and incubated in 96-well plates at 95 °C for 2 min, followed by 40 cycles of 95 °C for 5 s and 60 °C for 30 s using the ABI 7500 Fast Real-Time PCR Detection System (39). RT-quantitative PCR data were analyzed using the comparative threshold method and normalized to the expression of β-actin.

eNOS Activity Measurement. Isolated aortic ECs were stimulated with or without ACh (10 μM; 37 °C for 5 min) or CsA (10 nM, 100 nM, 1 μM; 37 °C for 1 h), followed by NOS activity assay detection (ENOS-100; BioAssay Systems). Briefly, 25 μL of cell lysates was mixed with 100 μL of NOS working reagent at 37 °C for 20 min to produce NO. NO production was then measured following reduction of nitrate to nitrite using the Griess method (data obtained at OD_{540}). Concentrations of cell lysates were determined by means of the Bradford assay. NOS activity was calculated as follows:

$$\text{NOS Activity} = \left(\text{OD}_{\text{sample}} - \text{OD}_{\text{blank}}\right) / (20 * \text{Slope} * \text{Concentration})(\text{U/g}).$$

Cell Culture. Pooled HUVECs were purchased from the American Type Culture Collection (ATCC) and cultured in vascular cell basal medium with the Endothelial Cell Growth Kit-BBE (ATCC). For knockdown experiments, scrambled or IP3R1 siRNAs were incubated with Lipofectamine 2000 Transfection Reagent (Thermo Fisher Scientific) and transfected into cells according to the manufacturer's instruction. Experiments were conducted after 72 h of transfection (47). Cells of passages 3–5 were used for all experiments.

Statistics. All results are presented as the mean ± SEM. Statistical analysis was performed using an unpaired two-tailed Student's *t* test unless otherwise indicated. *P* values less than 0.05 were considered significant.

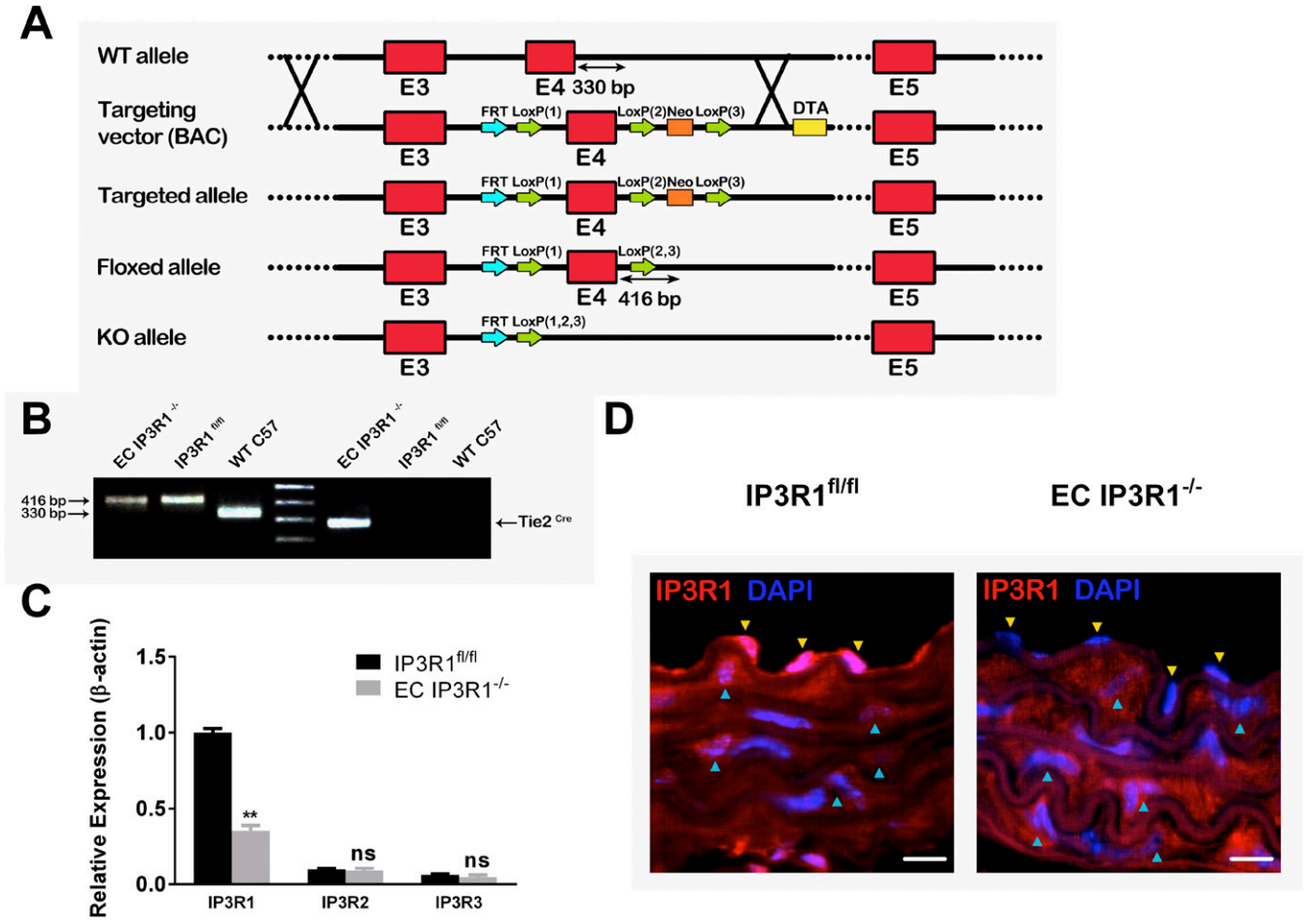

Fig. S1. Generation and characterization of EC IP3R1$^{-/-}$ mice. (*A*) Schematic diagram of the procedure for generating the EC IP3R1$^{-/-}$ mice. (*Top*) Wild-type (WT) *IP3R1* gene locus. Red boxes indicate exons 3–5. In the targeting vector, a loxP site was inserted at both sides of exon 4, followed by a phosphogylcerol kinase-gene neocassette and a diphtheria toxin A marker (DTA) inserted at the 3′ end of exon 4. A floxed allele was generated after deleting the neocassette. (*Bottom*) *IP3R1* KO allele obtained by crossing floxed mice with Tie2^{Cre} mice. (*B*) Representative genotyping PCR results from C57 WT (*Right*), IP3R1$^{fl/fl}$ (*Middle*), and EC IP3R1$^{-/-}$ (*Left*) mice. The 416-bp product indicates a floxed allele with loxP insertion. Tie2^{Cre} was also confirmed by PCR in KO mice. (*C*) IP3R subtype mRNA levels were evaluated by real-time RT-quantitative PCR from vascular ECs, using β-actin as an internal control. Values are shown as mean ± SEM of four independent experiments, each in triplicate. $^{**}P < 0.01$ compared with IP3R1$^{fl/fl}$, Student's *t* test. ns, not significant. (*D*) Representative immunofluorescence images of aortas from IP3R1$^{fl/fl}$ and EC IP3R1$^{-/-}$ mice stained for IP3R1 (red). Nuclei were counterstained with DAPI (blue). Yellow arrowheads indicate ECs beyond the inner elastic lamina, and blue arrowheads indicate smooth muscle cells surrounding ECs. (Magnification: 63×.) (Scale bars: 10 μm.)

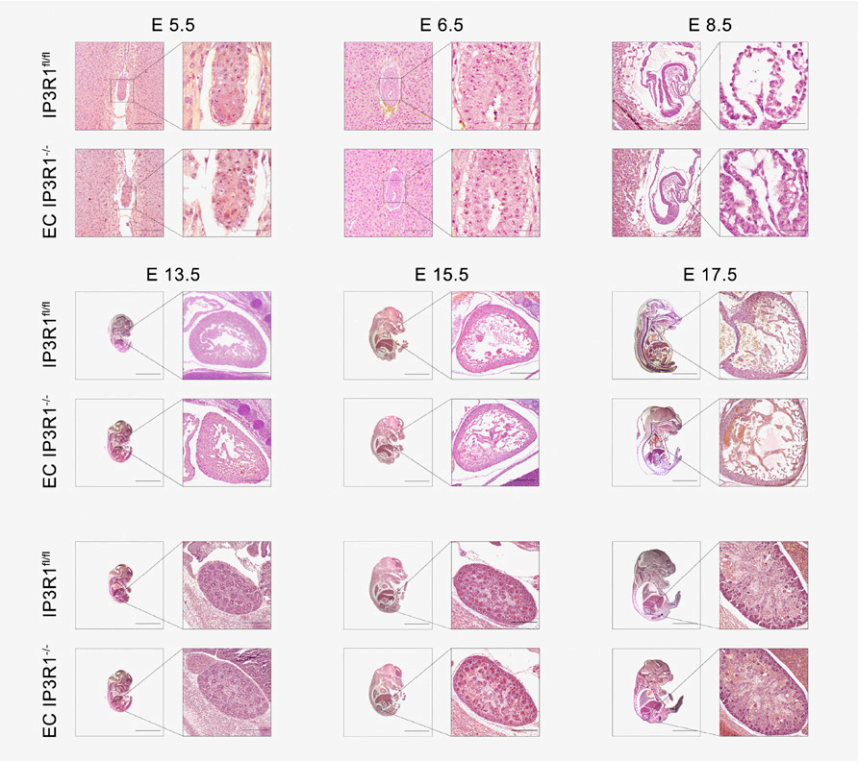

Fig. S2. Normal embryonic development of EC IP3R$^{-/-}$ mice. Pregnant IP3R1$^{fl/fl}$ and EC IP3R1$^{-/-}$ mice were killed, and embryos of embryonic day (E) 5.5, E 6.5, E 8.5, E 13.5, E 15.5, and E 17.5 were fixed and paraffin-embedded. H&E staining was conducted on sagittal sections of embryos. No abnormalities were found in EC IP3R1$^{-/-}$ embryonic development compared with IP3R1$^{fl/fl}$ embryos. [Scale bars: E 5.5 and E 6.5: 100 μm (zoom: 25 μm); E 8.5: 200 μm (zoom: 25 μm); E 13.5: 4 mm (zoom: 100 μm); and E 15.5 and 17.5: 4 mm (zoom: 200 μm).]

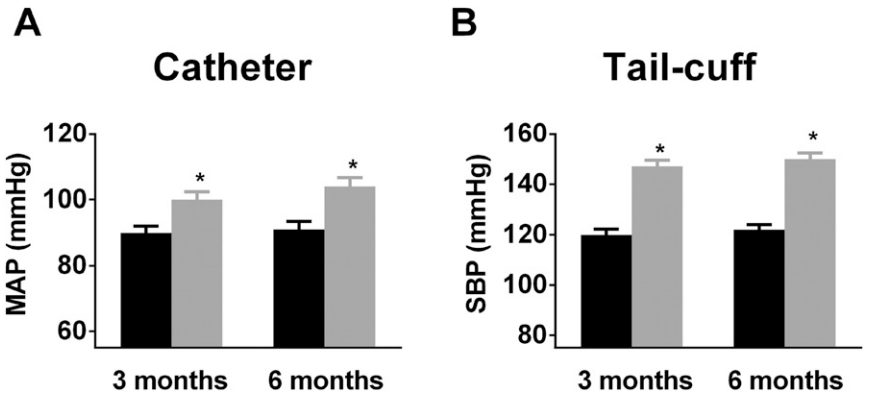

Fig. S3. BP measured by intra-arterial catheter and tail-cuff. (*A*) Mean arterial pressure (MAP) recorded by invasive catheter. (*B*) Systolic BP (SBP) was measured by tail-cuff and calculated in at least seven mice from IP3R1$^{fl/fl}$ and EC IP3R1$^{-/-}$ mice. All data are presented as mean ± SEM. *$P < 0.05$ vs. IP3R1 $^{fl/fl}$ mice by Student's *t* test.

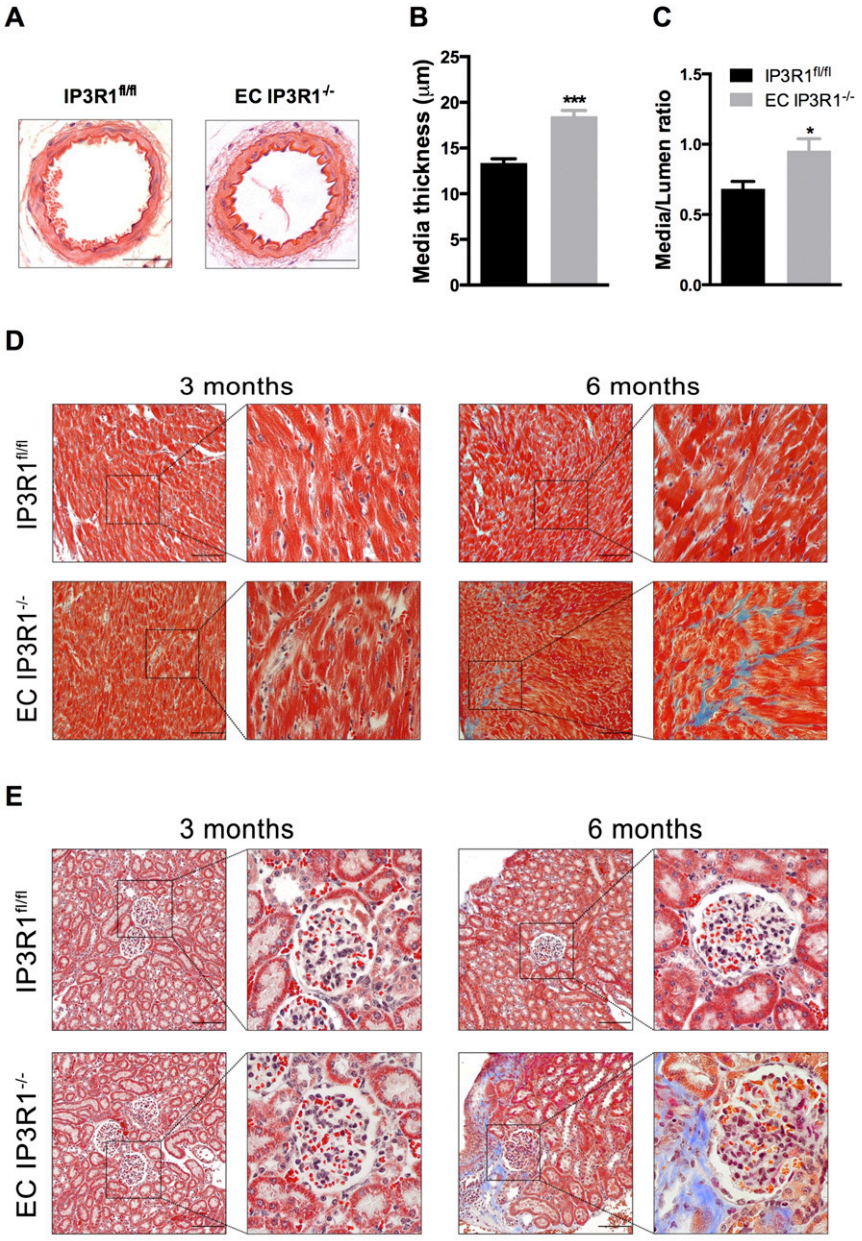

Fig. S4. Targeted end-organ damage in EC IP3R1$^{-/-}$ mice. (*A*) Representative pictures of H&E staining on paraffin-embedded mesenteric arteries of 6-mo-old IP3R1$^{fl/fl}$ and EC IP3R1$^{-/-}$ mice. Data statistics of media thickness (*B*) and media/lumen ratio (*C*) calculated from at least eight vessels of four individual mice per each group are shown. *$P < 0.05$; ***$P < 0.001$ vs. IP3R1$^{fl/fl}$ mice analyzed by Student's *t* test. Masson's trichrome staining on paraffin-embedded sections shows massive fibrosis (indicated by blue stain) of both the heart (*D*) and kidney (*E*) in 6-mo-old EC IP3R1$^{-/-}$ mice, which is hardly detected in IP3R1$^{fl/fl}$ littermates. (Scale bars: 50 μm.)

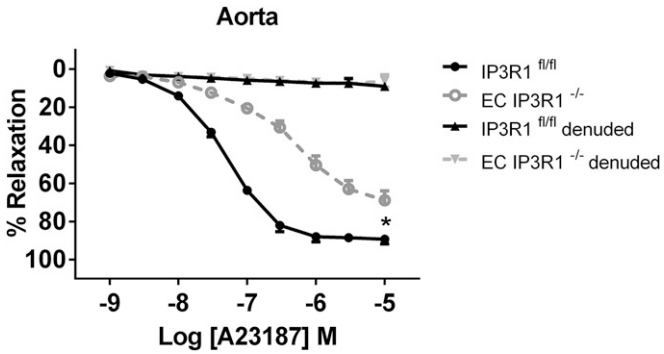

Fig. S5. Vascular reactivity in response to endothelium-dependent agonist A23187. Endothelium-dependent relaxation to A23187 in aortic segments. Data are presented as mean ± SEM (n = 4–8 rings from at least three mice per group). *$P < 0.05$.

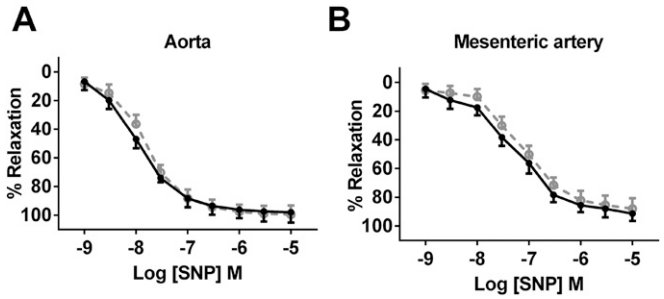

Fig. S6. Vascular reactivity in response to endothelium-independent agonist. (*A*) Endothelium-independent relaxation to SNP in aorta arteries. (*B*) Endothelium-independent relaxation to SNP in mesenteric arteries. Data are presented as mean ± SEM (n = 12–20 rings from six mice per group for aorta arteries, n = 8 for isolated mesenteric arteries).

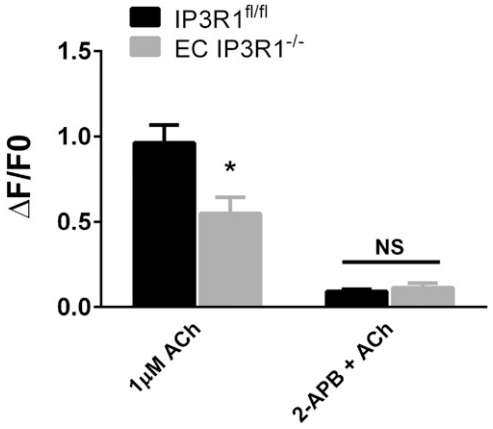

Fig. S7. Effect of 2-aminoethoxydiphenyl borate (2-APB) on ACh-induced $[Ca^{2+}]_i$ release. Summarized data of ACh-induced endothelial Ca^{2+} increase. Data are presented as mean ± SEM (n = 30–40 cells from six mice per each group). *$P < 0.05$.

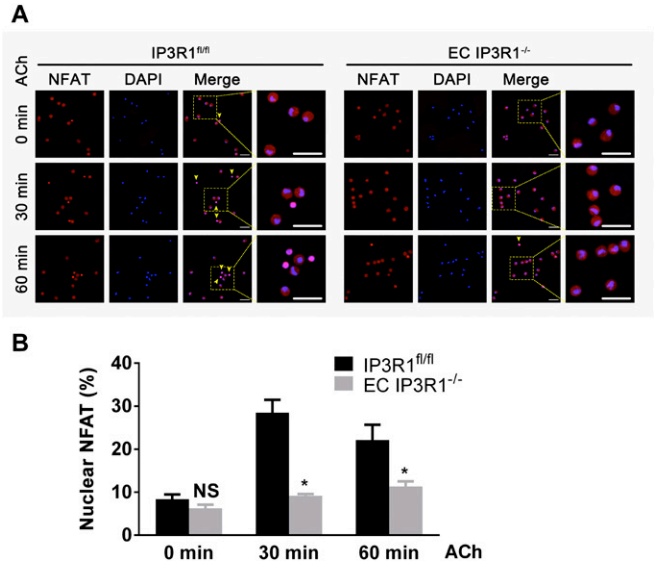

Fig. S8. NFAT translocation upon ACh stimulation in aortic ECs. (*A*) Representative immunofluorescence images of NFAT intracellular localization in time-dependent, ACh-treated aortic ECs. Yellow arrowheads indicate ECs with NFAT nuclear translocation. NFAT, red; DAPI, blue. (Magnification: 20×.) (Scale bars: 20 μm.) (*B*) Data statistics of percentages of cells with nuclear-translocated NFAT (translocated cell number/total cell number * 100%). More than 50 cells were calculated for each condition, and data are presented as mean ± SEM of three independent experiments. *$P < 0.05$; NS, not significant vs. IP3R1$^{fl/fl}$ ECs within the same group, analyzed by Student's *t* test.

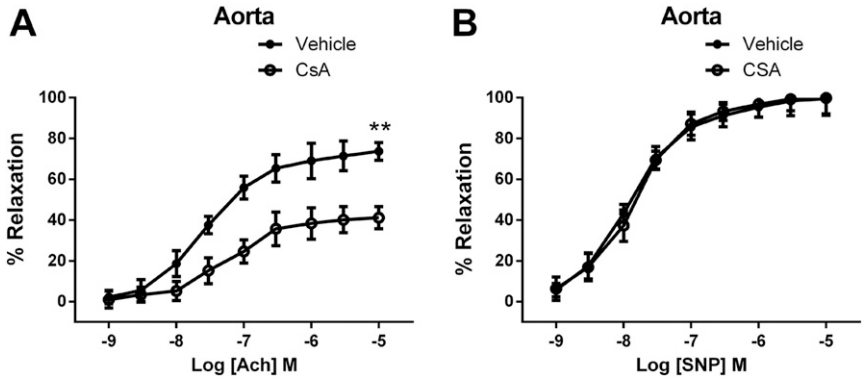

Fig. S9. Effect of CsA treatment on vascular reactivity. (*A*) Endothelium-dependent relaxation in response to ACh in aortic segments. (*B*) Endothelium-independent relaxation in response to SNP in aortic segments. Data are presented as mean ± SEM ($n = 8–12$ rings from three mice per group for aortic arteries). **$P < 0.01$.

Table S1. Characteristics of 3- and 6-mo-old IP3R1$^{fl/fl}$ and EC IP3R1$^{-/-}$ mice

	3 mo		6 mo	
Parameters	IP3R1$^{fl/fl}$	EC IP3R1$^{-/-}$	IP3R1$^{fl/fl}$	EC IP3R1$^{-/-}$
BW, g	24.1 ± 0.9	24.4 ± 1.2	25.6 ± 0.9	25.5 ± 1.3
HR, bpm	508 ± 48	506 ± 62	502 ± 52	510 ± 56
HW/BW, mg/g	4.02 ± 0.7	4.8 ± 0.8	4.03 ± 0.5	6.01 ± 0.8*
HW/TL, mg/mm	5.6 ± 0.8	5.9 ± 0.9	5.6 ± 0.9	7.7 ± 1.1*
EF, %	78.3 ± 3.2	77.8 ± 3.8	78.5 ± 3.6	61.2 ± 3.3*
IVS, mm	0.73 ± 0.05	0.75 ± 0.06	0.72 ± 0.04	0.89 ± 0.07*
LVPW, mm	0.72 ± 0.04	0.73 ± 0.03	0.71 ± 0.05	0.90 ± 0.05*

bpm, beats per minute; BW, body weight; EF, ejection fraction; HR, heart rate; HW, heart weight; IVS, interventricular septum; LVPW, left ventricular posterior wall; TL, tibial length. $n = 8–10$ mice per group.
*$P < 0.05$ vs. IP3R1$^{fl/fl}$.

Table S2. Primer sequences for real-time RT-quantitative PCR

Gene	Primer sequence	PCR product, bp
mIP3R1	F: ACCTTAGGCTTGGTTGATGAC	102
	R: AGGACATAGCTTAAAGAGGCAG	
mIP3R2	F: AGACTCTCAGCTCGCTCTGG	99
	R: GGCCACGACATCCTGTAACT	
mIP3R3	F: ACATCCTGGCTGAAGACACC	93
	R: AAAGGTCTCCACCTCCGTCT	
mβ-Actin	F: GATCAAGATCATTGCTCCTCCTG	183
	R: AGGGTGTAAAACGCAGCTCA	
hIP3R1	F: GTTAGAACTGAAGAACAATGCCTC	163
	R: TCCATCCTCAAATTCCACTTCAC	
heNOS	F: CCTGTGTATGGATGAGTATGAC	186
	R: CGGATCTTATAACTCTTGTGCTG	
hβ-Actin	F: AAGATCAAGATCATTGCTCCTCC	193
	R: TTGTCAAGAAAGGGTGTAACGC	

F, forward; h, human; m, mouse; R, reverse.